THIRTEENTH EUROPEAN ROTORCRAFT FORUM

12.6

Paper No. 72

ASPECTS AND RESULTS OF PROFILE DEVELOPMENT FOR CIRCULATION CONTROLLED ROTOR SYSTEMS

H. ZIMMER
DORNIER GMBH
FRIEDRICHSHAFEN, GERMANY

September 8-11, 1987
ARLES, FRANCE

ASSOCIATION AERONAUTIQUE ET ASTRONAUTIQUE DE FRANCE

ASPECTS AND RESULTS OF PROFILE DEVELOPMENT FOR CIRCULATION CONTROLLED ROTOR SYSTEMS*)

H. ZIMMER, DORNIER GMBH

ABSTRACT

In order to increase the flight speed of the helicopter and to prevent the advancing blade tip of becoming supersonic, the rotor turn rate has to be decreased. To maintain the lift on the retreating blade, most of which experiences onset flow from the rear, circulation controlled airfoil and rotor technology has been developed.

After a short discussion of the associated problems, a profile design for a high speed circulation controlled helicopter rotor system is described. A wind tunnel model with three interchangeable COANDA surfaces was built and measured in the low speed region. The results show a considerable improvement in the equivalent lift to drag ratio over known circulation controlled airfoils especially for positive angle of attack and high lift coefficients.

Finally the application of the developed airfoil to a high speed CCR-helicopter with propulsor is outlined.

NOTATION

ABC	Advancing Blade Concept
BERP	British Experimental Rotor Program
CCP(R)	Circulation Controlled Profile (Rotor)
c	Chordlength
$C_D = C_{DM} - C_\mu \frac{V_o}{V_j}$	Drag Coefficient
$C_{D,e} = C_D + C_\mu \frac{V_o}{V_j} + \frac{1}{2} C_\mu \frac{V_j}{V_o}$	Equivalent Drag of a CCP
C_{DM}	Drag measured with wake rake
C_L	Lift coefficient
C_{m50}	Half chord pitching moment coefficient
$c_\mu = 2 \frac{h}{c} (\frac{V_j}{V_o})^2$	Blowing momentum coefficient
c_p	Pressure coefficient
c_{p^*}	Critical pressure coefficient
D	Rotor diameter
D_p	Propulsor diameter
G	Aircraft weight
H	Height
H_T	Tail height of aircraft
h	Slot height
HOKUM	Code name of a military helicopter with coaxial rotor
ISA	International Standard Atmosphere
i	Gear reduction ratio
L	Fuselage length
L.E.	Leading Edge
M_T	Tip Mach number of the advancing blade
n	Rotor turn rate
n_V	Compressor turn rate
P	Power
P_c	Compressor power
P_{max}	Maximum installed power
$P_{max\ cont}$	Maximum continuous power
P_R	Rotor shaft power
R	Radius of the rotor, local radius of the COANDA surface
R_{ec}	Reynolds number relative to the chord length
T	Rotor thrust
T.E.	Trailing edge
U	Circumferential velocity
U_1	Velocity at the outer edge of the boundary layer
V, V_o	*Flight velocity, onset velocity*
V_j	Blowing jet velocity
W_n	Local onset velocity normal to the blade leading edge
x,y,z	Rectangular coordinate system
x_s	Blowing slot position
α	Angle of attack
δ	Boundary layer thickness
θ_o	Collective pitch setting of the rotor
$\mu = \frac{V}{u}$	Advance ratio
ψ	Circumferential angle
ω	Turning frequency

*) This study was conducted under contract Nr. T/RF 41/F0013/G2232 [1]

1. INTRODUCTION

Most of todays helicopters use a single main rotor which generates lift, propulsion and attitude control. Yaw control and compensation of the rotor torque is provided by the tail rotor the axis of which is arranged normal to the direction of flight. Since these helicopters have special mission capabilities their further development is of interest.

E.g. the hover performance of these helicopters is optimal, but in view of flight speed and range they are less efficient than comparable fixed wing airplanes. Therefore all over the world efforts are undertaken in order to improve the helicopter performance, e.g. by higher harmonic control, improved blade airfoils and special tip shapes.

While these possibilities are explored on conventional rotor systems, also alternative rotor systems are examined in order to improve the helicopter performance. To reach this goal basically the advance ratio limit has to be overcome. Since the rotational speed is superimposed with the forward velocity the rotor flow is unsymmetric as is shown in FIG. 1 for a typical conventional helicopter. The rotor is turning around the momentary pole Mp. In this figure the advance ratio limit is reached with $\mu = .35$. Above this limit the retreating blade cannot afford any more the required lift because of the partial separated flow.

With the special tip shape according to FIG. 2 left side [2] the helicopter speed record was broken in Aug. 1986 with a speed of 216 kts. By these tips a high Mach Number of the advancing blade tip is possible ($M_T = 0,97$) and on the retreating side a high angle of attack ($\alpha = 20°$), so that in the outer rotor region the separation is delayed according to FIG. 2 right side [3]. But also in this case the advance ratio limit is about $\mu = 0,35$.

2. PROBLEM DEFINITION

In order to further increase the flight speed, the advancing blade tip Mach number has to be decreased (which means also less noise emission). Therefore alternative rotor systems have to be taken into consideration in order to overcome the advance ratio limit:

a) The counter rotating coaxial high speed rotor (ABC-Rotor, FIG. 3, HOKUM). Here the flow asymmetry is compensated by the second counterrotating rotor and so the advance ratio limit is avoided.

b) The tilt rotor concept (XV-3, XV-15, V-22, FIG. 4, EUROFAR) consists of two tilt rotors arranged at the wing tips of a fixed wing aircraft. Here the advance ratio limit is circumvented by tilting the rotor axis into the direction of the incoming flow. So the rotors are acting as propellers in axial flow.

c) The third alternative rotor system, the X-Wing concept according to FIG. 5, overcomes the advance ratio limit by using a CCR with leading and trailing edge blowing. So the local lift generation is possible in forward and reversed flow. At a certain transition speed the rotor shall be stopped and acts now as a fixed X-Wing.

The object in view of the present study is a helicopter with a flight speed between that of the conventional helicopter and that of the tilt rotor concept at about 250 kts. The hover performance of the conventional helicopter and also the relatively simple mechanical system with a single main and tail rotor should be retained. Also the complexity should not be far away from that of an advanced conventional helicopter.

3. EVALUATION WITH REGARD TO THE PRESENT OBJECT IN VIEW

A short evaluation of the rotor systems mentioned above with regard to the object in view of the present study was made. Since the advance ratio will be about 0.75 and even more, a conventional rotor system would not be feasible because the retreating blade would be almost entirely in reversed flow. Also special blade tip forms would be of no effect, since they were in nearly static condition on the retreating side.

For this advance ratio range a coaxial rotor system would be possible. But because of the high drag of the advancing load carrying blades a thrust producing device is needed for the envisaged speed regime (s. FIG. 3). Because of the relatively heavy and complex system consisting of two rotors and a propulsion unit this rotor system was not further considered in this study. For a less demanding velocity requirement of around 200 kts the counter rotation coaxial rotor system is feasible without propulsor (HOKUM).

The tilt rotor concept (FIG. 4), which is capable of a flight speed of around 300 kts with a certain disadvantage in hover performance in comparison with that of the conventional helicopter, has already reached a high development standard. But with its two tiltable rotors and the additional wing this rotor concept is also relatively heavy and complex and was not considered further in the present study.

The X-Wing concept shall combine the advantages of the fixed wing aircraft (efficient cruise flight in the Mach 0.8 flight regime), with the advantages of the conventional helicopter (efficient hovering). But this is only possible by a stoppable circulation controlled rotor with an extreme stiffness in the rotor head and the blades. Also convertible engines are needed which can operate as turboshaft and turbofan engines and also a complex flight control system. Therefore also this rotor concept is considered as too heavy and two complex for the present study.

4. PROPOSED ROTOR CONCEPT

The rotor concept envisaged in the present study shall combine the proven features of the CCR-technology with the relative simplicity of the conventional helicopter with a single main and tail rotor. As can be seen on FIG. 6 a helicopter configuration with an aerodynamically clean fuselage, a bearingless flex beam CCR is considered. The tailrotor is reconfigured as a propulsor with its axis in flight direction. Yaw control and rotor torque compensation is achieved by two rudders in the propulsor down wash, also an elevator is integrated.

FIG. 7 shows the dependence of flight speed, circumferential speed and advancing blade tip Mach number, and in FIG. 8 the regions with reversed flow on the rotor disk are shown in dependence of advance ratio. The cruise flight design point is point A in FIG. 7 with an advance ratio of 0.75 at a flight speed of 250 kts. The advancing blade tip Mach number is about 0.89. For this point in FIG. 9 the lines of equal relative total head are shown.

In the shaded area the total head relative to the total head of the circumferential velocity is less than 1/16. In this region only a small portion of the lift force can be generated (compare also FIG. 13). In order to use the reversed flow in this region, the CCR-technology is needed. In FIG. 10 [4] the control of such a rotor is shown in principle by blowing over the leading and trailing edges of the blades in dependence of the circumferential blade position. In quadrant I and III the main part of the lift is generated (compare also FIG. 13). In the advancing quadrant II the blowing has to be reduced in order to maintain the rolling moment equilibrium with the quadrant IV, with reversed flow in the inner region. Therefore here additionally leading edge blowing has to be used.

5. DEVELOPMENT OF CIRCULATION CONTROLLED AIRFOILS

The performance of a CC-rotor depends strongly on the performance of the used CC-profiles. These profiles have a thick rounded trailing edge, the COANDA surface, over which a thin two dimensional jet is blown tangentially. This jet follows the COANDA surface a certain distance until it separates in dependence of several parameters. This kind of circulation control is most effective since with a relatively small amount of blowing a relatively high change of the off-flow direction from the trailing edge of the airfoil and hence circulation and lift increase can be achieved.

Since the first publications on CC-profiles (e.g. [5]) a rapid development of the CC-aerodynamics took place (e.g. [6], [7]). As is shown in FIG. 11 these airfoils exhibit quite a high equivalent lift to drag ratio at high lift coefficients. At low lift coefficients the conventional airfoils are better. This figure shows also the possible margin between simple and advanced CC-profiles for comparison. From FIG. 12 [8] the conclusion can be drawn, that in quadrant III, where dual edge blowing is needed according to FIG. 10, also high lift coefficients can be achieved. In the present study the known state of the art in circulation control profile aerodynamics is taken as a starting point. Then it was tried to design an improved airfoil by applying design principles which proved earlier to be efficient in transonic airfoil design [9]. Of decisive importance for the profile design are the calculation methods used. In [1] the calculation procedure used in the present study is described in more detail. Here only an outline of the method is given.

6. CALCULATION OF CC-PROFILES

FIG. 13 [8] shows the lift distribution of a CC-rotor in fast forward flight at an advance

ratio of 0.85. The statistical distribution of the blade loading in this case with respect to section Mach number and angle of attack, which can be seen in FIG. 14 [8], shows the fact that the main part of the rotor lift is generated at very small mach numbers. Therefore the profile calculations are made so far with an incompressible theory. Only for the wall jet calculation a compressibility correction is applied.

The calculation method used in the present study is based on [10]. It was generalised in such a manner, that general airfoil shapes with a general COANDA surface can be treated [1]. In the calculation procedure a potential flow theory (conformal mapping by a FOURIER series development, THEODORSSEN-method) is coupled with a boundary layer method. The boundary layer equations according to L. PRANDTL are solved by the CEBECI-SMITH finite difference scheme on the upper and lower surface of the airfoil. As can be concluded from FIG. 15 first the potential flow pressure distriubtion is calculated for a given lift coefficient. Then for this condition the lower surface boundary layer development is calculated up to the lower separation point which yields a certain separation pressure coefficient $c_{p\ ABL,U}$. Then the upper surface boundary layer is calculated up to the blowing slot position. If no separation has occurred the boundary layer properties at the position of the slot and the blowing jet conditions are the starting conditions for the wall jet calculation. This is done by solving the simplified time averaged NAVIER-STOKES equations by the KELLER-CEBECI finite difference scheme with appropriate outer boundary conditions and turbulence modeling [1]. Then the wall jet is calculated up to the upper separation point with a certain separation pressure coefficient $c_{p\ ABL,O}$. The basic velocity profile types on the COANDA surface are shown in FIG. 16. Near the blowing slot a velocity minimum is evident which stems from the mixing of the upper boundary layer and the blowing jet. Further downstream the velocity profiles show a maximum near the COANDA surface which stems from the jet momentum.

Generally the two calculated separation pressures $c_{p\ ABL,U}$ and $c_{p\ ABL\ O}$ are different. But in order to have a physically meaningful working condition the two pressures have to be equal according to the THWAITES condition [1], which takes the place of the KUTTA-JOUKOWSKY condition on conventional airfoils.

Therefore the blowing jet momentum has to be varied in an iterative procedure, until the two separation pressures are equal for the required lift coefficient. The flow diagram of the calculation procedure with the described three major calculation steps is shown in FIG. 17.

There is experimental evidence [11] that the wall jet pressure ratio should be lower than critical. For a higher pressure ratio an over-expansion of the jet on the COANDA surface takes place. The associated shocks and expansion waves disturb or destroy the COANDA-effect. Therefore the COANDA effect works best with a subcritical jet pressure ratio and so a relatively simple compressibility correction to the wall jet yields reasonable results [1] (s. FIG. 33).

7. CALCULATION OF THE KIND AIRFOIL

First the KIND Airfoil [12] was calculated. This example is of special interest, since the velocity distributions were measured in the wall jet. FIG. 18 shows the profile geometry and the pressure distribution for the considered working point. The wall jet theory shows the influence of the blowing jet on the pressure distribution of the COANDA surface. Also the two calculated separation points are evident. As can be seen on this figure and also in FIG. 19 the separated flow region is quite large on this airfoil (14 % of the chord length). On FIG. 19 the positions are shown were the calculated velocity profiles are compared with the measurement. FIG. 20 depicts the starting velocity profile for the wall jet calculation (A), also the velocity profile at the lower separation point (B) and FIG. 21 shows the velocity profiles on the COANDA surface. The calculated values compare quite well with the measurement. A further improvement of the results is only possible by solution of the Reynolds number averaged NAVIER-STOKES equations [13].

8. AIRFOIL DESIGN

After an overview of the aerodynamic characteristics of the known CC-profiles the airfoil design was carried out mainly with the aim of

a) a low suction peak on the upper surface of the airfoil nose in order to delay the leading edge separation

b) a separation region as small as possible on the lower surface at the trailing edge in order to minimize the drag.

In order to fulfill a) a nose camber is introduced and to fulfill b) the airfoil is designed such, that on the rear lower surface the potential pressure distribution does not show the progressive pressure rise up to the stagnation pressure as in FIG. 18 but a short distance before the trailing edge an acceleration should take place. These features were already applied successfully in the design of the transonic airfoil according to FIG. 22 [9]. They result in a M-shaped airfoil mean line with the associated front and rear loading.

The starting point for the present CC-profile was an advanced cambered 15 % thick CC-profile [14], on which the above mentioned design principles were applied. The designed airfoil together with its flow field and pressure distribution for zero angle of attack without blowing is shown in FIG. 23. Here the described acceleration phase at the trailing edge is evident. In order to save computer time, the design calculations were made without boundary layer and wall jet. The blowing was simulated by prescribing the rear stagnation point and an additional super velocity on the COANDA surface simulating the wall jet. An example of this calculation is given in FIG. 24. Here the high suction peak on the COANDA surface is evident. In order to achieve the most efficient blowing effect, the slot location should be a small amount upstream of the potential flow suction peak of the COANDA surface. Of such calculations as shown in FIG. 24 the slot position was fixed at 96 % chord length as is shown in FIG. 25.

This figure shows also the three different COANDA surfaces which were designed. Besides the circular surface with a radius of 3,3 % chordlength (DOCCP CIR) a spiral type (DOCCP SPI) and an elliptical type (DOCCP ELL) COANDA surface were designed.

The potential flow field around these different trailing edges is shown in FIG. 26 for a lift coefficient of 3. According to this calculation the spiral type trailing edge a) with the strong camber immediately upstream the trailing edge seems to be adapted in the best way to the local flow field. The contrary seems to be true for the elliptical type trailing edge.

9. MEASUREMENT

A wind tunnel model of the designed airfoil with the chord length of 0.6 m was built according to FIG. 27 with the three interchangeable trailing edges according to FIG. 25. The model installed in the wind tunnel can be seen in FIG. 28. The measurement was done for different slot heights and different blowing momentum coefficients. For the test set up, data reduction, complete data set see [1] and the references there. The trend expected according to FIG. 26 was verified by the measurement and the airfoil with spiral type trailing edge yielded the best results. (Compare also FIG. 11).

9.1 Total Force and Moment Coefficients

The total force and moment coefficients for the profile DOCCP SPI are shown on FIG. 29-31 for a slot height h/c = 0.0013. FIG. 29 depicts the lift coefficient in dependence of angle of attack and blowing momentum coefficient. A maximum lift coefficient of 3.9 is achieved. FIG. 30 shows the drag and FIG. 31 the half chord pitching moment characteristics. In these figures the points are given, at which calculations with boundary layer and wall jet were made. Generally a very good agreement was found, even for the drag calculation according to FIG. 30.

9.2 Pressure Distributions

Two examples of the pressure distriubtion are given. In FIG. 32 the measured values at zero angle of attack without blowing are compared with the calculation (Point 1). When the theoretical pressure distribution of FIG. 32 is compared with FIG. 23 the theoretical influence of the boundary layer is evident in the reduction of the lower rear pressure peak. The measured pressure distribution in FIG. 32 shows also the acceleration region but not so strong as it is in the calculation.

The pressure distribution of point 4 (FIG. 29) is shown in FIG. 33. Generally the correlation between measurement and calculation on the lower surface is very good, also the separation pressure and the extension of the separated flow region are exactly predicted. In this case the separation region has a length of about 7 % of the chord length and is about half that of FIG. 18. The height of the suction peak on the COANDA surface is well predicted by the wall jet theory when the compressibility is taken into account. The development of the wall jet on the COANDA surface can be seen on FIG. 34. Point 16 is the separation point.

9.3 Equivalent lift to drag ratio

Of great practical interest is the equivalent lift to drag ratio in dependence of lift coefficient (comp. also FIG. 11). FIG. 35 shows the experimental results of the best airfoil for different angles of attack. In the equivalent drag a term is included, which accounts for the compressor power associated with the blowing jet momentum. So different airfoils can be compared directly.

10. PROFILE COMPARISON

FIG. 36 shows the measured equivalent lift to drag ratios at -3,1° angle of attack for the airfoil with the different COANDA surfaces. Here the degradation in performance from the spiral type over the circular to the elliptical type is evident (comp. FIG. 26).

In this figure also the results of the comparable airfoils according to [15] and [16] are shown. Only the designed airfoil with spiral type trailing edge reaches an equivalent lift to drag ratio of 34.

Finally FIG. 37 shows the envelopes of the equivalent lift to drag ratio for the considered airfoils. For lift coefficients above 1 a considerable improvement over the known state of the art has been achieved with a maximum value of 58. For comparison also the lift to drag ratio of an advanced conventional airfoil is shown [17]. From these results the conclusion can be drawn, that above a lift coefficient of 1.6 the equivalent lift to drag ratio of a CC-profile cannot be surpassed any more by a conventional airfoil.

11. APPLICATION

The three dimensional rotor flow and the required power of a CCR were calculated with the aid of a Curved Lifting Line Blade Element Vortex Wake method based on [18] with the local aerodynamic profile characteristics in dependence of the effective angle of attack, blowing momentum coefficient and Mach number as shown in FIG. 38 for an outer definition airfoil.

The mathematical model of the rotor flow field is shown for a hover case in FIG. 39 and FIG. 40 depicts the rotor wake model in a fast forward flight case with reversed onset flow over the complete span of the retreating blade. From such calculations and other considerations the most efficient blade configuration for the present application is derived and presented in FIG. 41. The designed airfoil is at the 75 % radius position and the blade is designed such, that the tip region with the highest Mach number and small positive and negative lift coefficients consists of a swept tip with 13 % thick symmetrical elliptical airfoils. Towards the blade root the shown M-shaped profile mean line becomes more and more pronounced, and inside the 60 % radius position also leading edge blowing is provided.

The hover performance of the rotor, the dimensions of which were chosen according to the design requirements of FIG. 43, is shown in FIG. 42 for different collective pitch settings. The rotor shaft power and the compressor power is shown separately. For the design weight (5 to) of the proposed CCR-helicopter (FIG. 44) the total required power in hovering is nearly 1000 kW with roughly one third accounting for compressor power. Of special interest is the comparison with the measurement of the XH-2 CCR demonstrator rotor [20]. Here the required power is higher for the same thrust. But this result is reasonable because of the smaller rotor diameter (FIG. 42).

An essential feature of the proposed CCR-helicopter (FIG. 44) is the propulsor, which is shown in FIG. 45. It consists of a high performance pusher propeller [18] [19] integrated at the rear fuselage. Two rudders for rotor torque compensation and yaw control are provided in the propeller down wash. Also the elevator is integrated in a high position in order to be clear of the main rotor down wash and to minimize the influence on the propeller. A big alleviation for this design is the fact that the rotor torque which has to be compensated is only about two thirds the value of a conventional rotor, and that the highest deflection of the propeller down wash is only needed in hover and at very low speed. But here the required propulsor power is only very low (see FIG. 48). For high propulsor power and high flow stagnation pressure practically no down wash deflection is needed.

The drive system of the proposed configuration is shown in FIG. 46. A main feature consists in the fact that the power for the compressor and the propulsor does not enter the main rotor gear box which therefore can be a lighter design than that of a conventional helicopter with only about two thirds of the power to be transmitted. So the additional weight for the compressor and the heavier propulsor drive train can be compensated for if possible.

In FIG. 47 a section through the rotor head, the main rotor gear box and the pneumatic control system is shown. The bearingless flex beam rotor head with mechanical collective pitch control is evident. A pneumatic control device according to the double segmented ring valve principle is shown and also a quadrant control system according to the slide valve principle (inset, [1] and references). This promising system allows higher harmonic control with only 5 actuators and contributes to a substantial reduction in complexity.

FIG. 48 shows the required total power, propulsor and compressor power of the proposed CCR-helicopter in dependence of flight speed and also the total required power of a conventional helicopter of the same weight and installed power. The comparison with this helicopter was chosen because the CCR-demonstrator [20] (s. FIG. 42) was based on this type. The power comparison according to FIG. 48 shows that the CCR-helicopter is capable of a nearly 100-kts velocity increase for maximum continuous power.

On FIG. 49 the performance summary is given. The range requirement can only be fulfilled for a weight increase of 5 %. The maneuverability summary of FIG. 50 finally shows a very high acceleration capability for the CCR-helicopter.

12. REFERENCES

1. A. Weigand, H. Zimmer, Ergebnisse der Profilentwicklung für fortschrittliche zirkulationsgesteuerte Rotorsysteme schneller Hubschrauber, DGLR Jahrestagung, Berlin, Oct. 1987.

2. F.J. Perry, Helicopter Rotor Blade, US Patent 4427344, Jan. 24, 1984.

3. B. Wanstall, Mit neuen Rotorblättern schneller als 200 Knoten, INTERAVIA 3, 1986, 322-324.

4. K.R. Reader, D.G. Kirkpatrick, R.M. Williams, Status Report on Advanced Development Program Utilizing Circulation Control Rotor Technology, 4th European Rotorcraft Forum, Stresa, Italy, Paper No. 44, Sept. 1978.

5. I.C. Cheeseman, The Application of Circulation Control by Blowing to Helicopter Rotors, Journal of the Royal Aeronautical Society, Vol. 71, No. 679, July 1967.

6. R.J. Engler, M.B. Stone, M. Hall, Circulation Control - An updated Bibliography of DTNSRDC Research and Selected Outside References, DTNSRDC Report 77-0076, Sept. 1977.

7. J.N. Nielsen, J.C. Biggers, Recent Progress in Circulation Control Aerodynamics, AIAA-Paper No. 87-0001, Jan. 1987.

8. E.O. Rogers, A.W. Schwarz, J. Abramson, Applied Aerodynamics of Circulation Controlled Airfoils and Rotors, 11th European Rotorcraft Forum, Paper No. 31, London, Sept. 1985.

9. E. Stanewsky, H. Zimmer, Entwicklung und Windkanalerprobung von drei überkritischen Tragflügelprofilen für Verkehrsflugzeuge, Z. Flugwiss. 23 (1975), Heft 7/8, 246-256.

10. E.H. Gibbs, N. Ness, Analysis of Circulation Controlled Airfoils, West Virginia University, Department of Aerospace Engineering, WV 26506, Aerospace Engienering TR-43, June 1975.

11. N.J. Wood, J.A. Conlon, The Performance of a Circulation Control Airfoil at Transonic Speeds, AIAA Paper No. 83-0083, Reno, USA, Jan. 1983.

12. R.J. Kind, D.J. Maull, An experimental Investigation of a Low-Speed Circulation Controlled Airfoil, The Aero. Quart., Vol. XIX, 170-182, May 1968.

13. G.D. Shrewsbury, Analysis of Circulation Control Airfoils Using an Implicit NAVIER-STOKES Solver, AIAA Paper No. 85-0171, Jan. 1985.

14. T.C. Tai, G.H. Kidwell, Numerical Optimization of Circulation Control Airfoil at High Subsonic Speed, J. Aircraft, Vol. 22, No. 10, Oct. 1985.

15. J. Abramson, Two-Dimensional Subsonic Wind Tunnel Evaluation of two Related Cambered 15 % Thick Circulation Control Airfoils, DTNSRDC/ASED Report 373, Sept. 1977.

16. J. Abramson, Low-Spoeed Characteristics of a Circulation Control Airfoil with Aft Camber and a Spiral Trailing Edge, DTNSRDC/ASED Report 84/97, Dec. 1984.

17. D. Welte, Profilentwurf für einen Tragflügel neuer Technologie für Flugzeuge der Allgemeinen Luftfahrt, Vortrag Nr. 77-027, DGLR-Jahrestagung, Berlin, 1977.

18. H. Zimmer, The Aerodynamic Calculation of Counter Rotating Coaxial Rotors, 11th European Rotorcraft Forum, London, Sept. 10-13, 1985.

19. H. Zimmer, R. Hoffmann, K.H. Horstmann, Investigation of Modern General Aviation Propellers, AGARD-CP-366, 1984.

20. J.B. Wilkerson, D.R. Barnes, F.A. Bill, The Circulation Control Rotor Flight Demonstrator Test Program, American Helicopter Society, Washington D.C., May 1979.

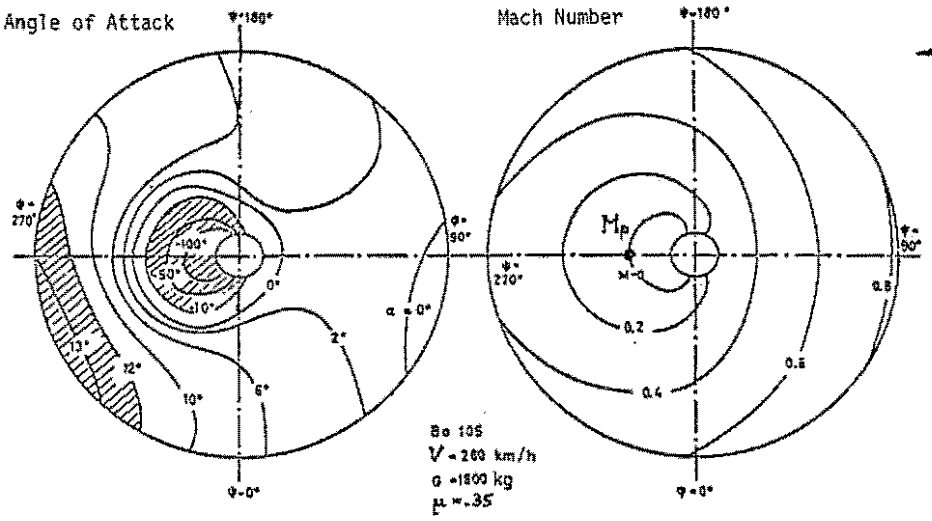

FIG. 1:
Angle of attack and Mach Number Distribution of a conventional helicopter at maximum speed. Regions with separated flow are shaded

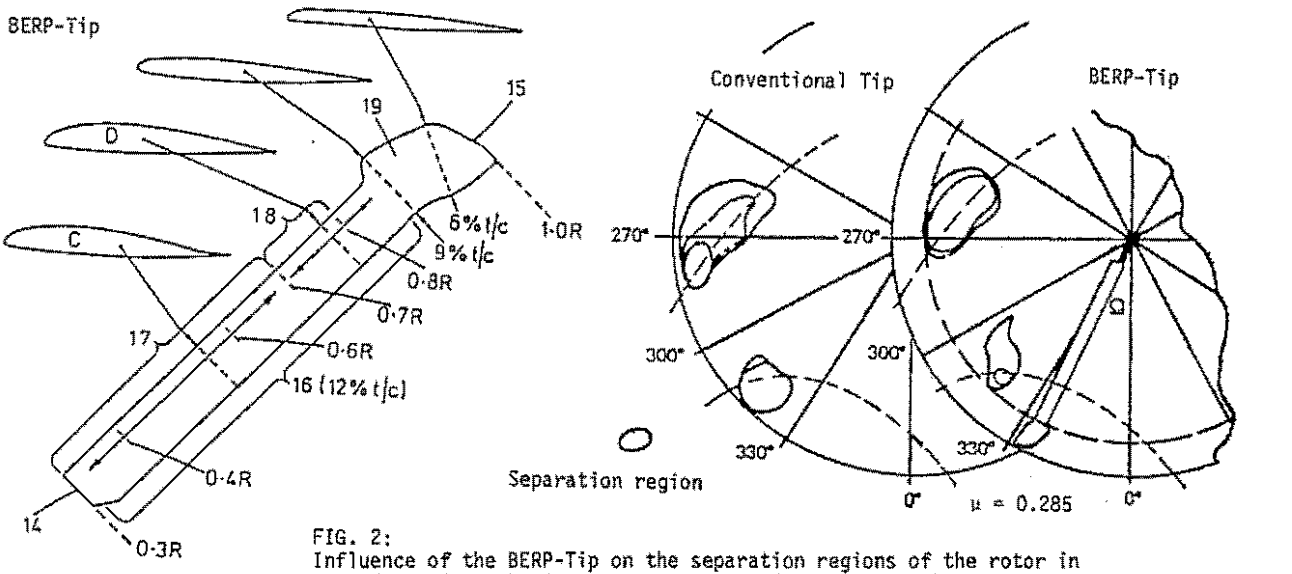

FIG. 2:
Influence of the BERP-Tip on the separation regions of the rotor in fast forward flight (no separation outside 0.85 radius).

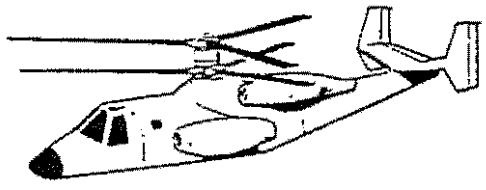

FIG. 3: ABC-Rotor

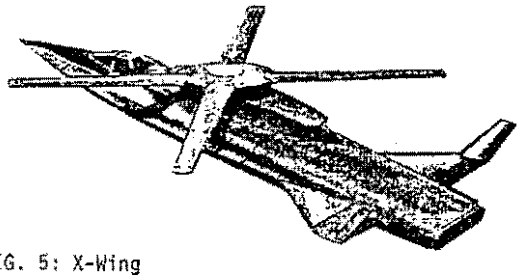

FIG. 5: X-Wing

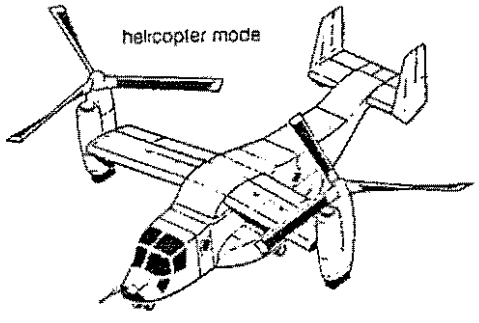

FIG. 4: Tilt Rotor

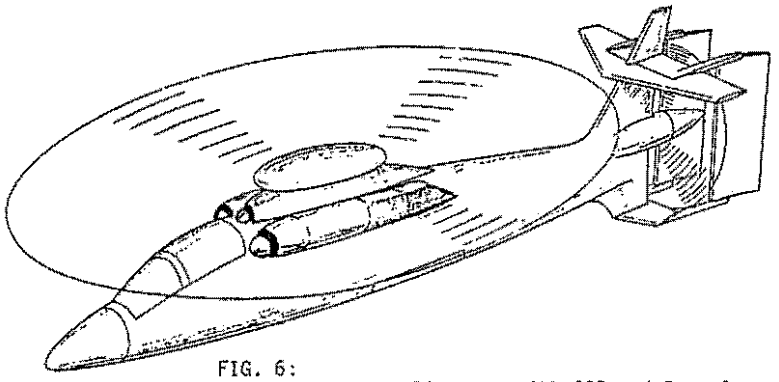

FIG. 6:
New Technology Helicopter with CCR and Propulsor

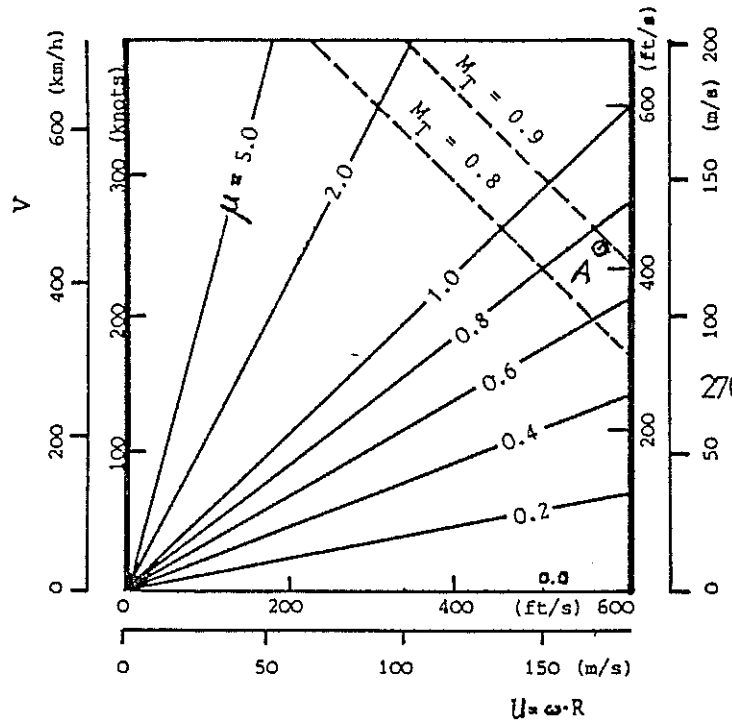

FIG. 7:
Advance Ratio in dependence of flight speed V, circumferential speed U and tip Mach number M_T

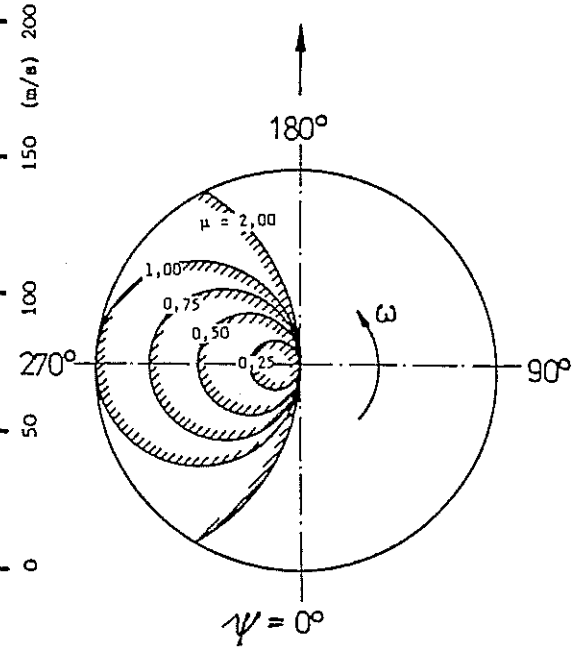

FIG. 8:
Regions with reversed flow (shaded) in dependence of advance ratio

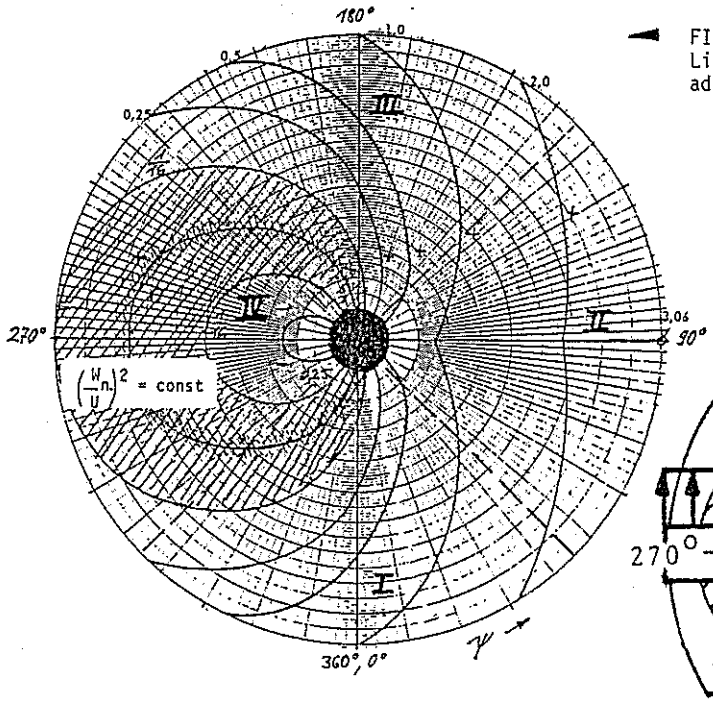

FIG. 9:
Lines of equal relative total head for the advance ratio μ = 0,75 (Point A in FIG. 7)

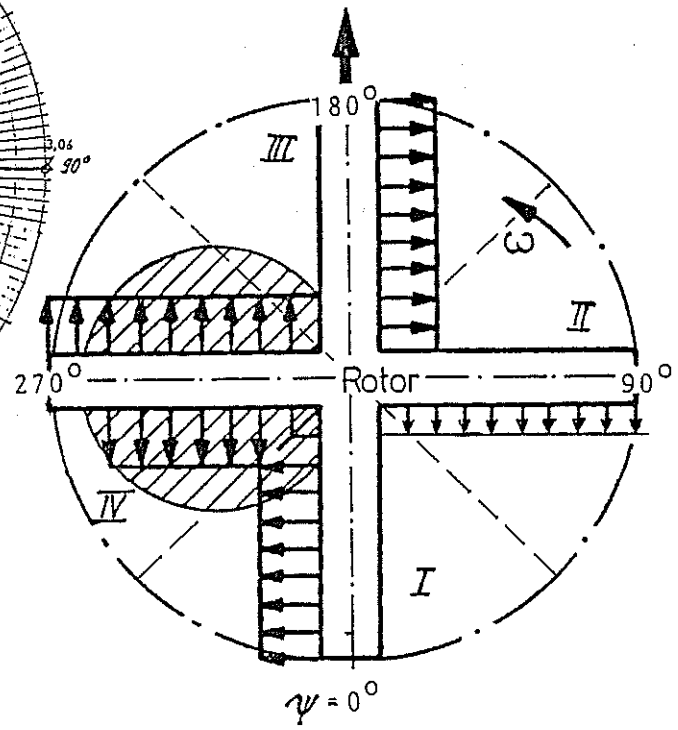

FIG. 10:
Control of a CCR by blowing over the leading and trailing edges in dependence of the circumferential blade position

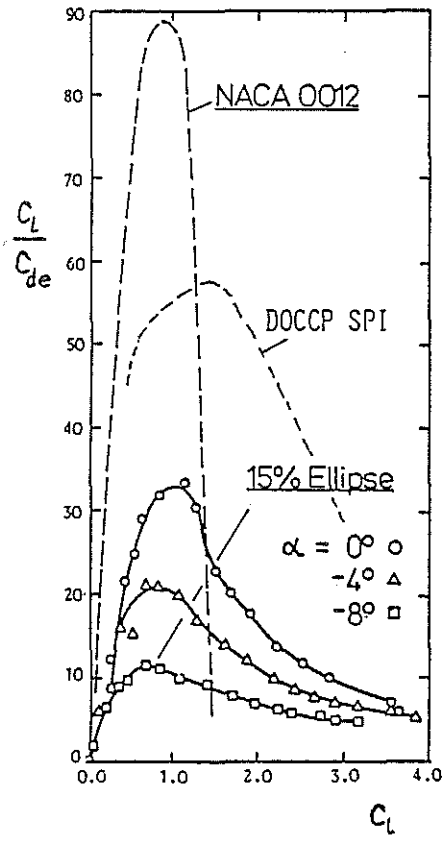

FIG. 11:
Comparison of the equivalent lift to drag ratio of a simple (ellipse) and an advanced (DOCCP SPI) CC-profile with a conventional airfoil

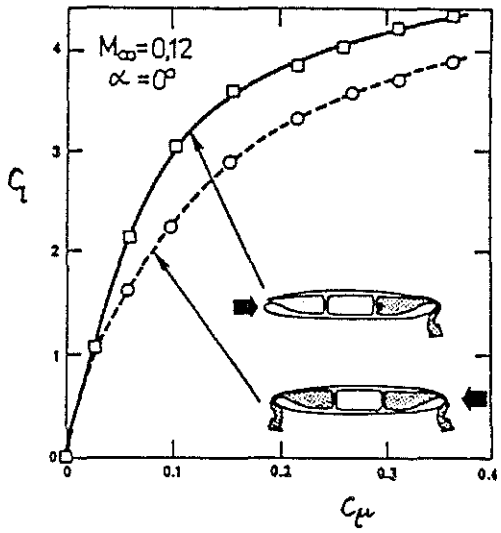

FIG. 12:
Comparison of the lift characteristics of a CC-profile with single and dual edge blowing

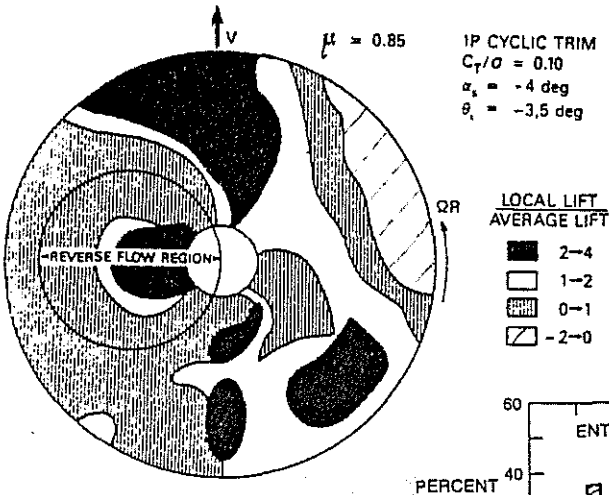

FIG. 13:
Load distribution of a CC-Rotor at an advance ratio of μ = 0,85

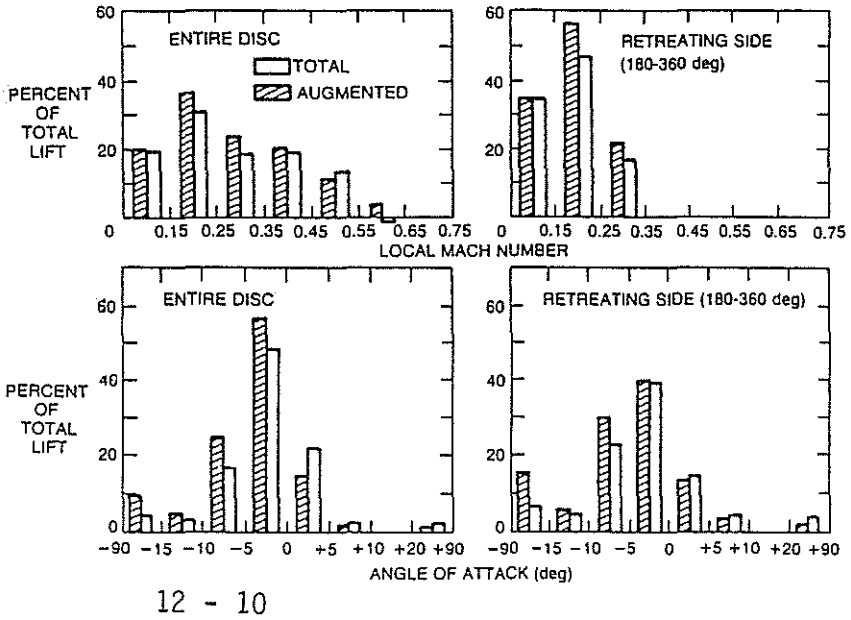

FIG. 14:
Statistical distribution of blade loading with respect to section Mach number and Angle of Attack

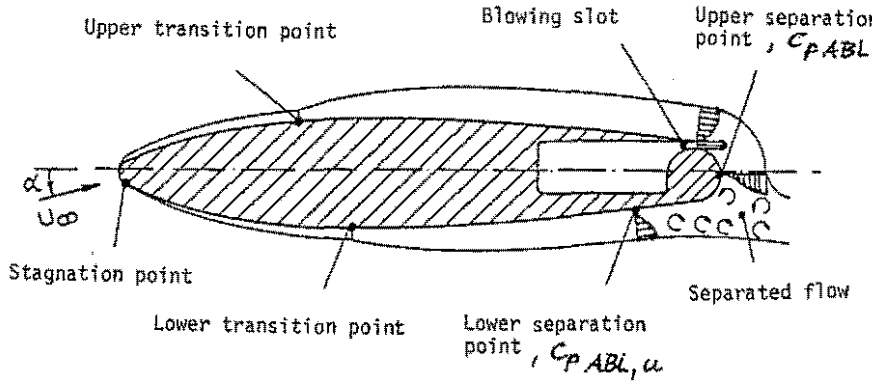

FIG. 15:
Boundary layer development on a CC-Profile
with transition and separation points

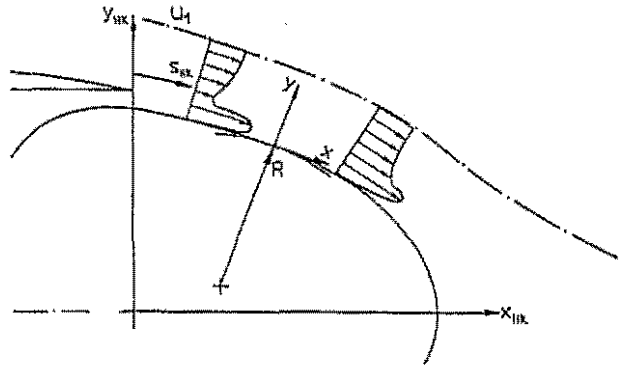

FIG. 16:
Geometrical properties and types of velocity profiles on the COANDA surface

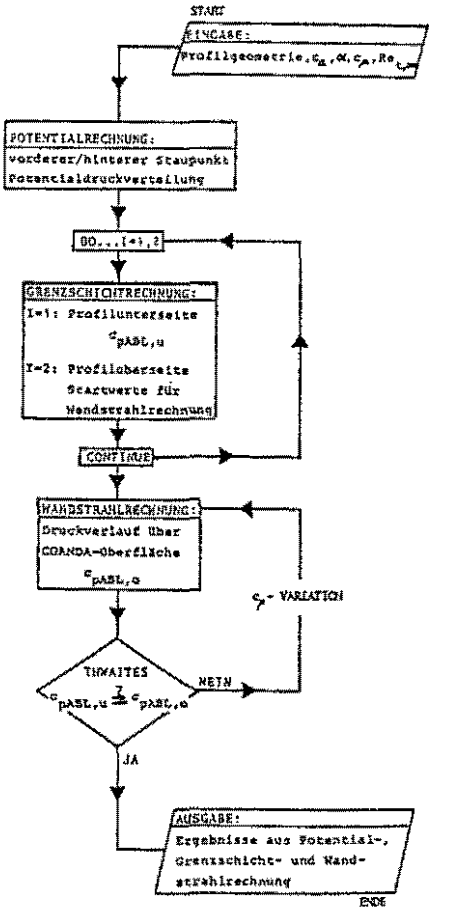

FIG. 17:
Flow Diagram of the computation Method

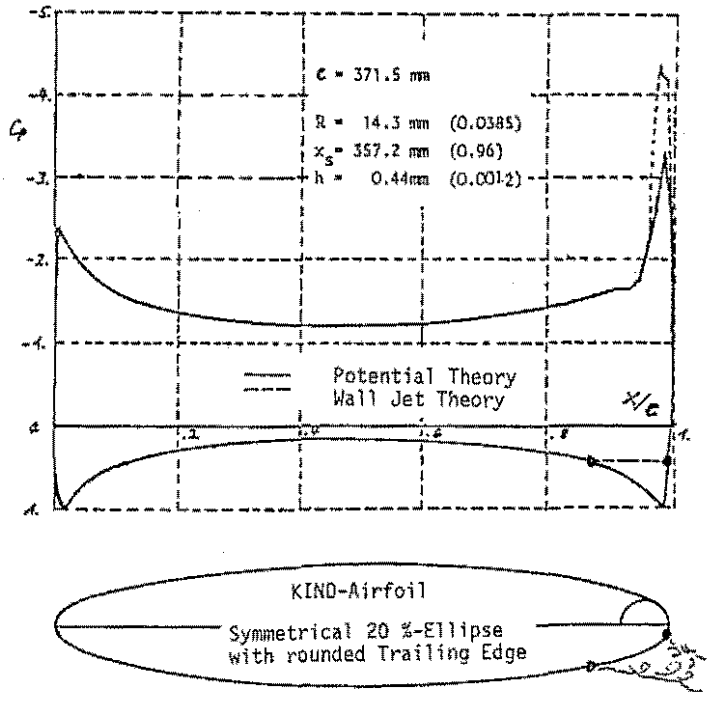

FIG. 18:
Pressure Distribution of the KIND-Airfoil for
C_L = 1,82; α = - 0,7°; C_μ = 0,054

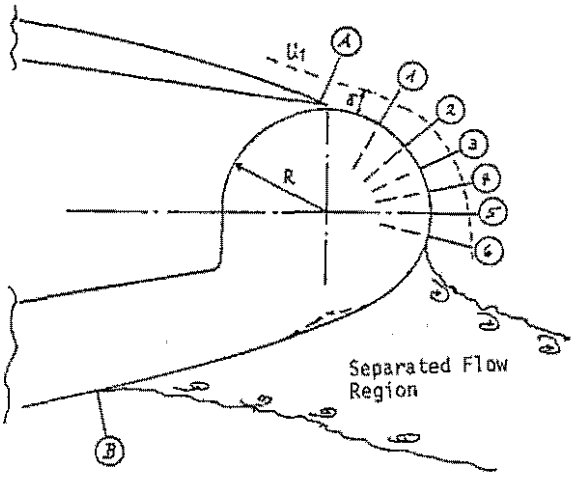

FIG. 19:
Position of the velocity profiles for the Boundary Layer and Wall Jet Calculation of the KIND-Airfoil according to FIG. 18

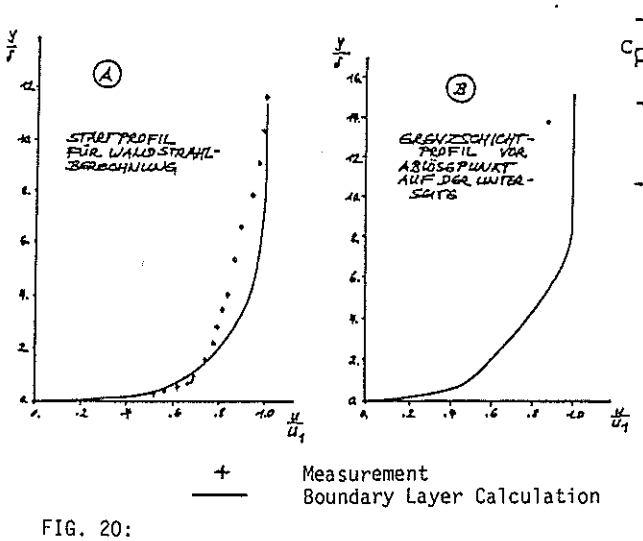

FIG. 20:
A: Starting Velocity Profile for the Wall Jet Calculation
B: Velocity Profile at the Lower Separation Point

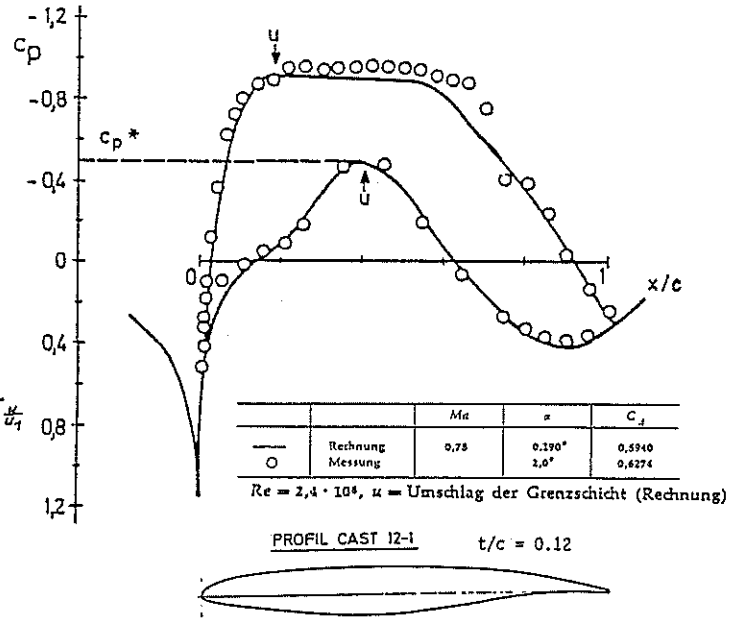

FIG. 22:
Pressure Distribution of the CAST 12-1 Airfoil in the Design Condition
(u = Transition Point)

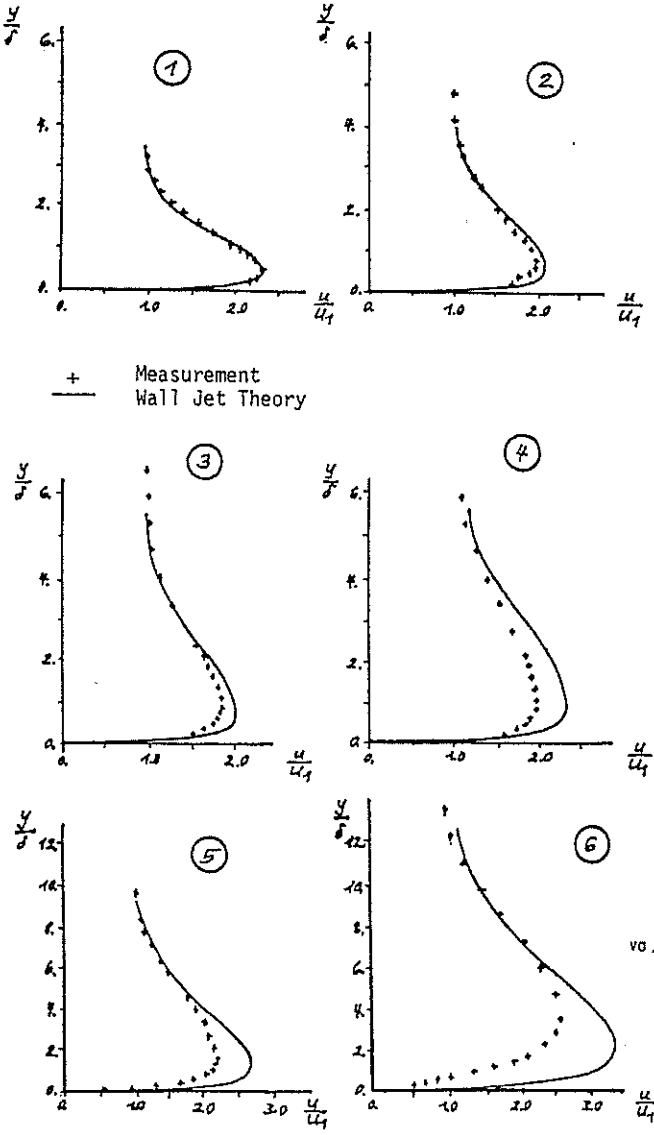

FIG. 21:
Velocity Profiles on the COANDA Surface of the KIND-Airfoil for the case according to FIG. 18

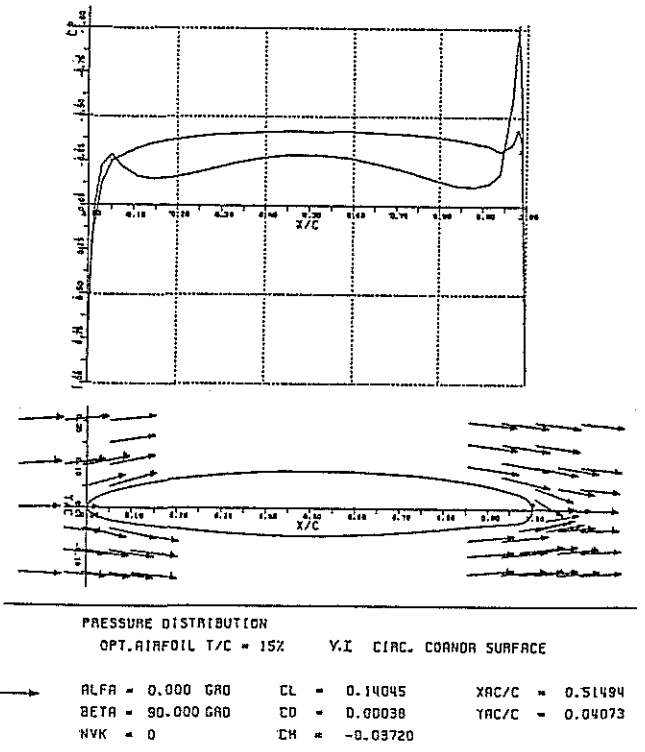

FIG. 23:
Potential Flow Pressure Distribution and partial Flow Field of the designed Airfoil at zero Angle of Attack without Blowing

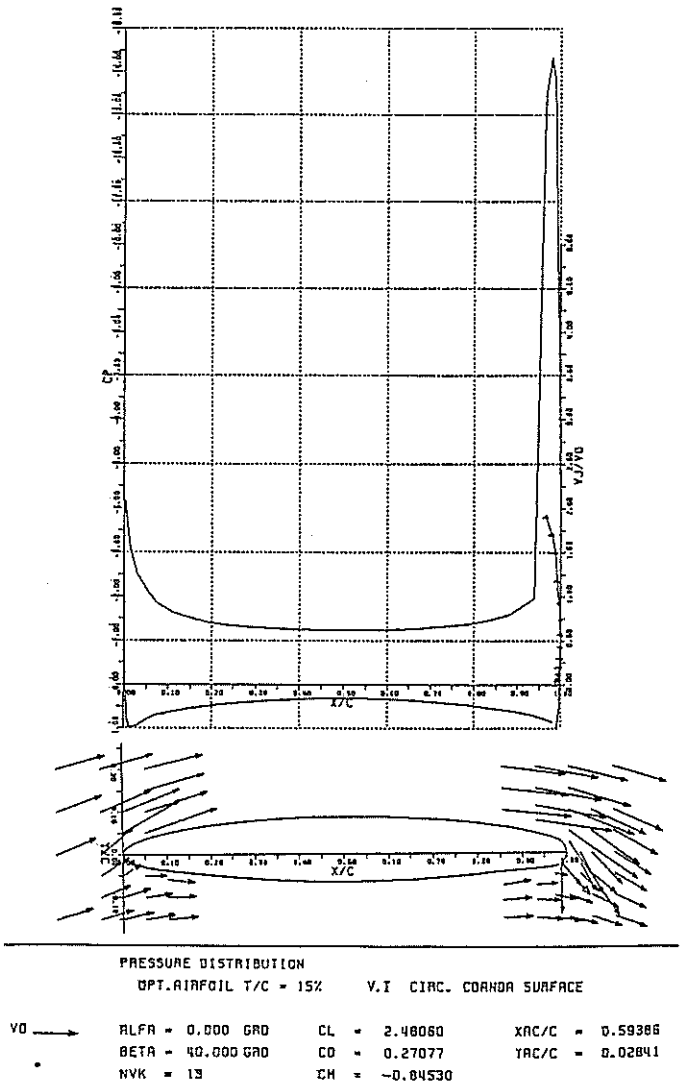

FIG. 24:
Potential Flow Pressure Distribution and Flow Field of the designed Airfoil at zero Angle of Attack and simulated Blowing

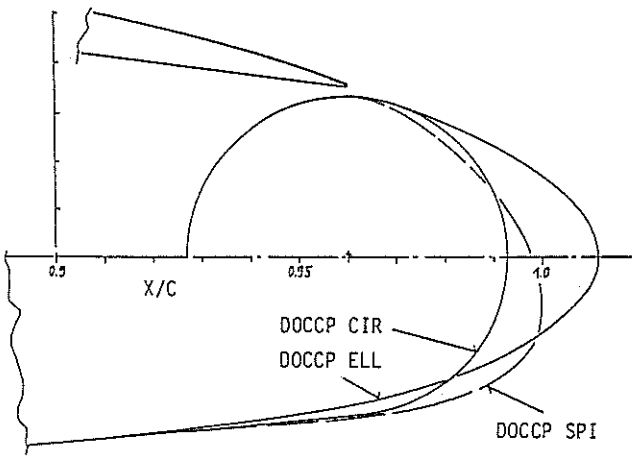

FIG. 25:
The three different COANDA-Surfaces of the designed Airfoil

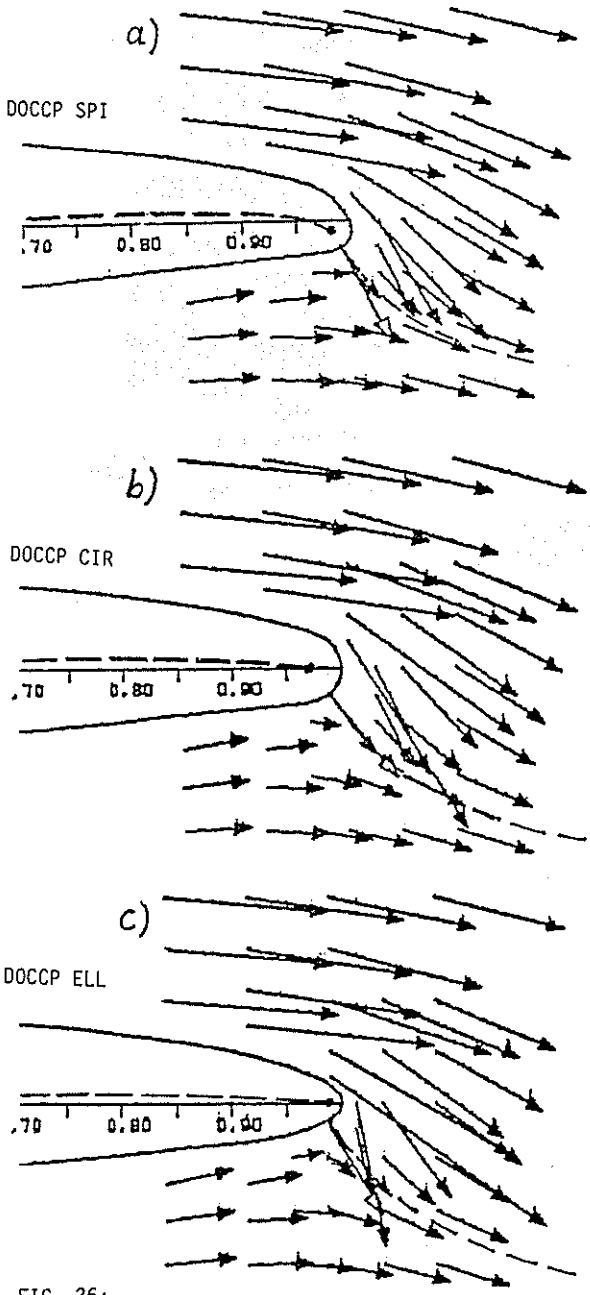

FIG. 26:
The Potential Flow Field near the three different Trailing Edge of the Designed Airfoil for Simulated Blowing, $\alpha = 6°$; $C_L \approx 3{,}0$

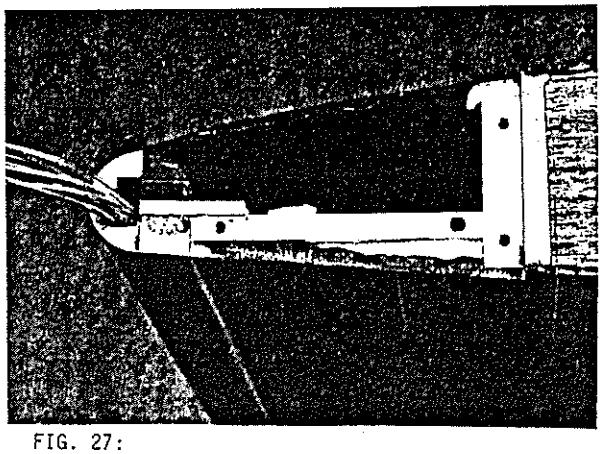

FIG. 27:
The Wind Tunnel Model (DOCCP CIR) (c = 0,6 m) with pressure measurement tubes

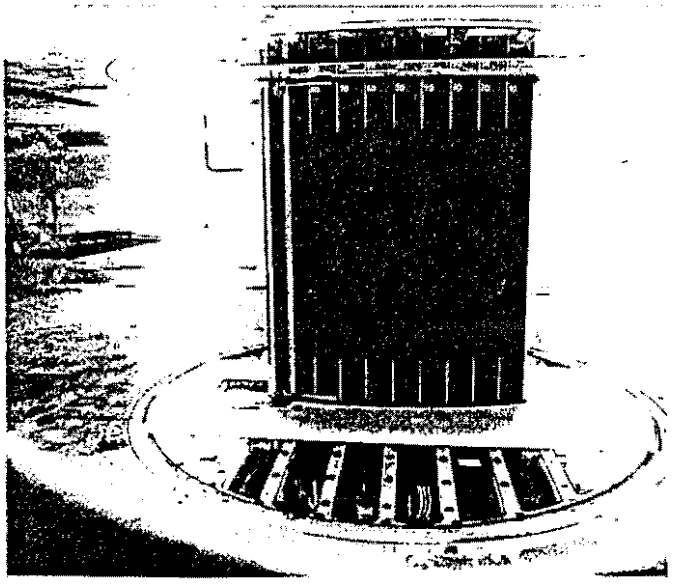

FIG. 28:
The model in the Laminar Wind Tunnel of the University of Stuttgart (c = 0,6 m; span = 0,728 m). The flow is from right to left, the wake rake is visible at left.

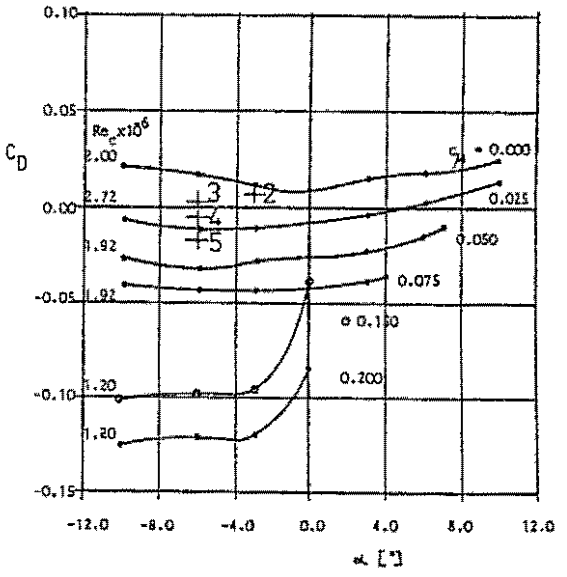

FIG. 30:
Measured Drag Characteristics of the profile DOCCP SPI and calculated points with Boundary Layer and Wall jet theory

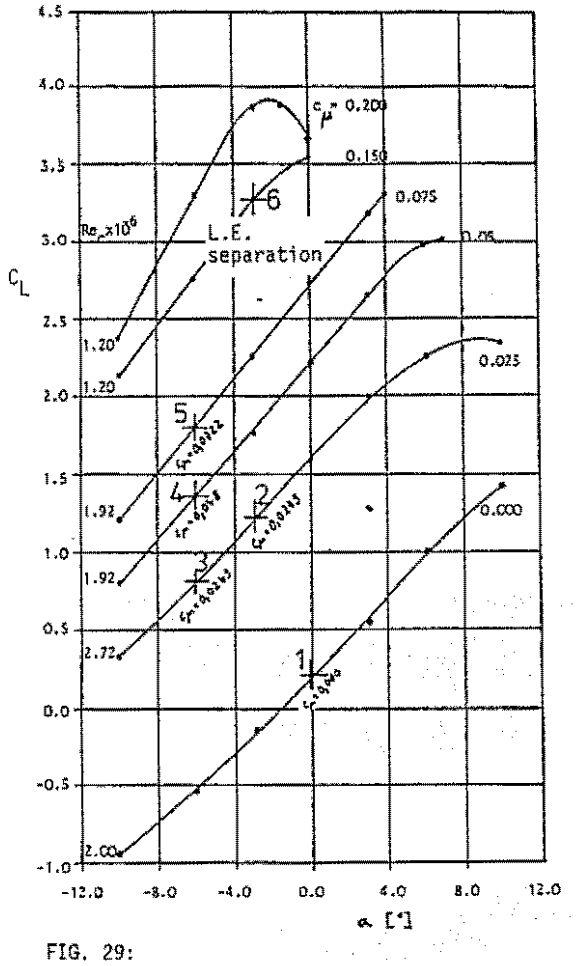

FIG. 29:
Measured lift characteristics of the profile DOCCP SPI and calculated points with Boundary Layer and Wall jet theory

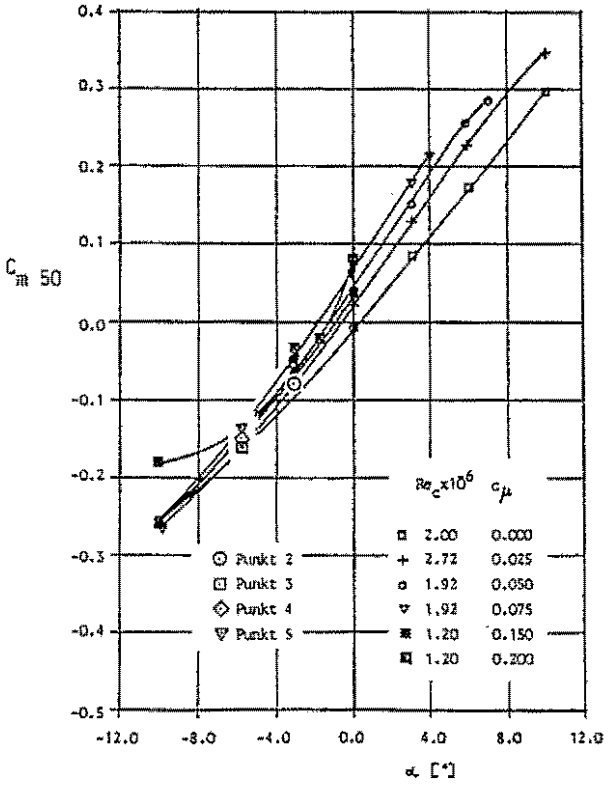

FIG. 31:
Measured half chord moment characteristics of the profile DOCCP SPI and calculated points with Boundary layer and Wall jet theory

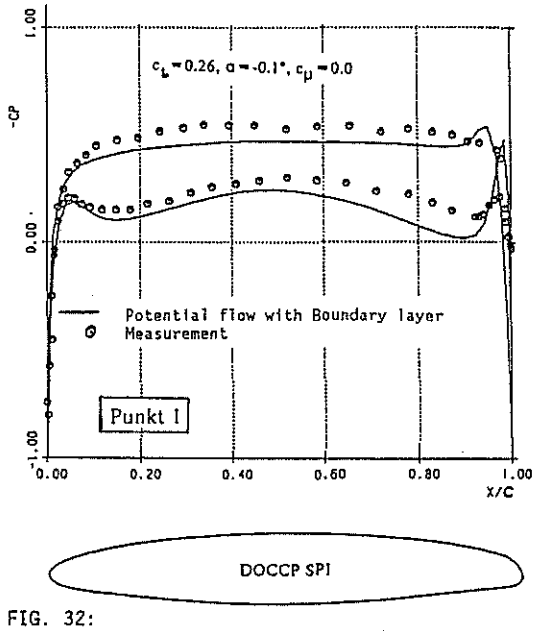

FIG. 32:
Comparison of the pressure distributions in Point 1 of FIG. 29 to 31

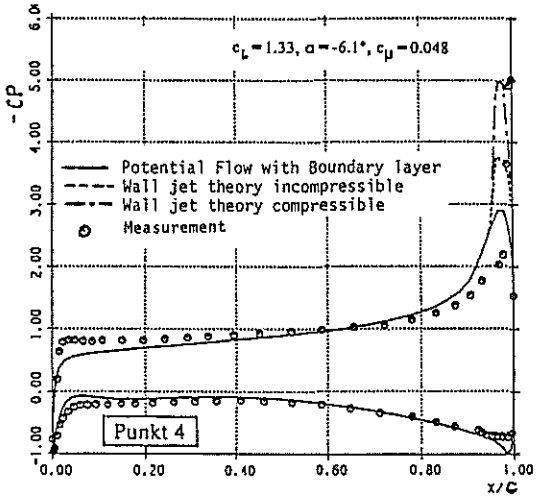

FIG. 33:
Comparison of the pressure distributions in Point 4 of Fig. 29 to 31

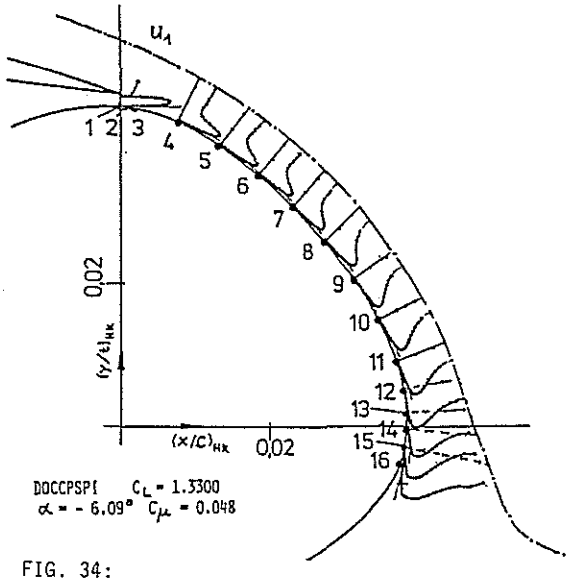

FIG. 34:
Theoretical velocity profiles in the Wall jet of the profile DOCCP SPI in Point 4

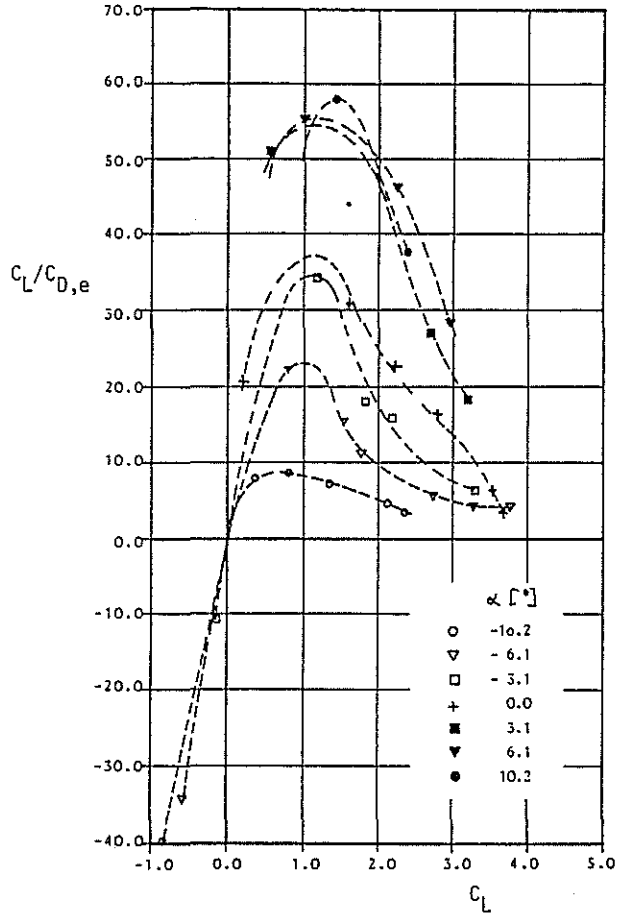

FIG. 35:
Equivalent lift to drag ratio of the profile DOCCP SPI with the slot height h/c = 0,0013 (h = 0,8 mm) at different angles of attack

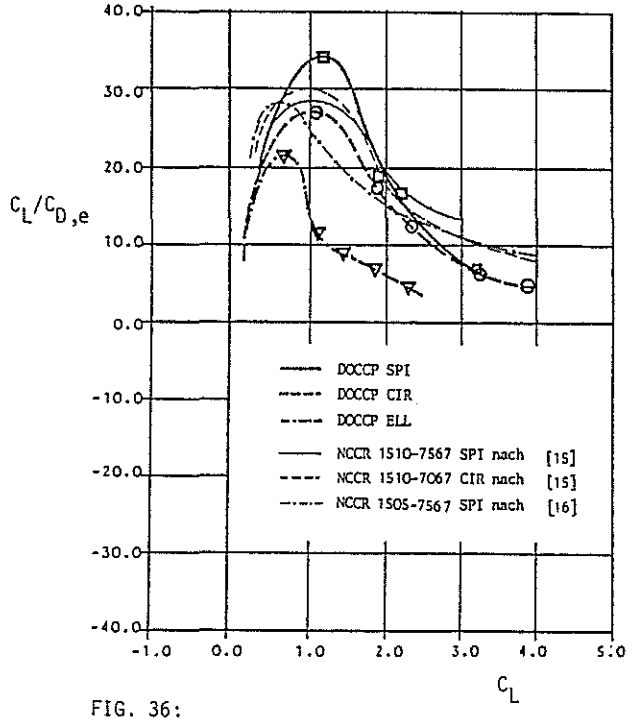

FIG. 36:
Comparison of the equivalent lift to drag ratio for different CC-profiles at the angle of attack of α = - 3,1°

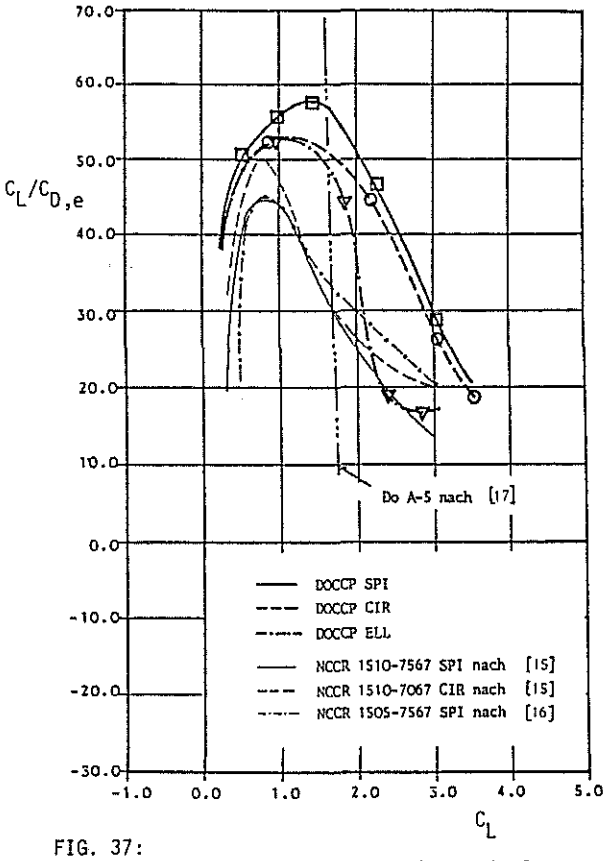

FIG. 37:
Comparison of the envelopes of the equivalent lift to drag ratio for different CC-profiles and an advanced conventional airfoil

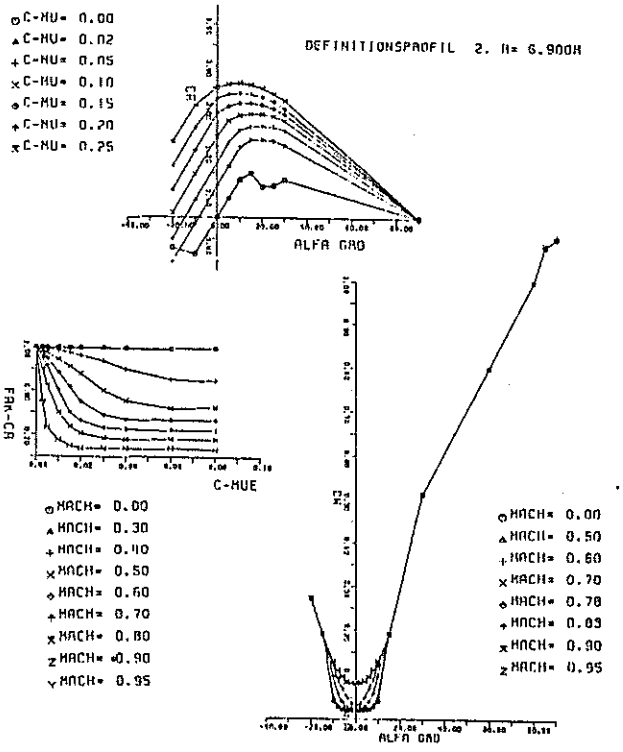

FIG. 38:
Lift and drag characteristics of a definition airfoil in dependence of blowing coefficient and Mach number for the threedimensional rotor calculation

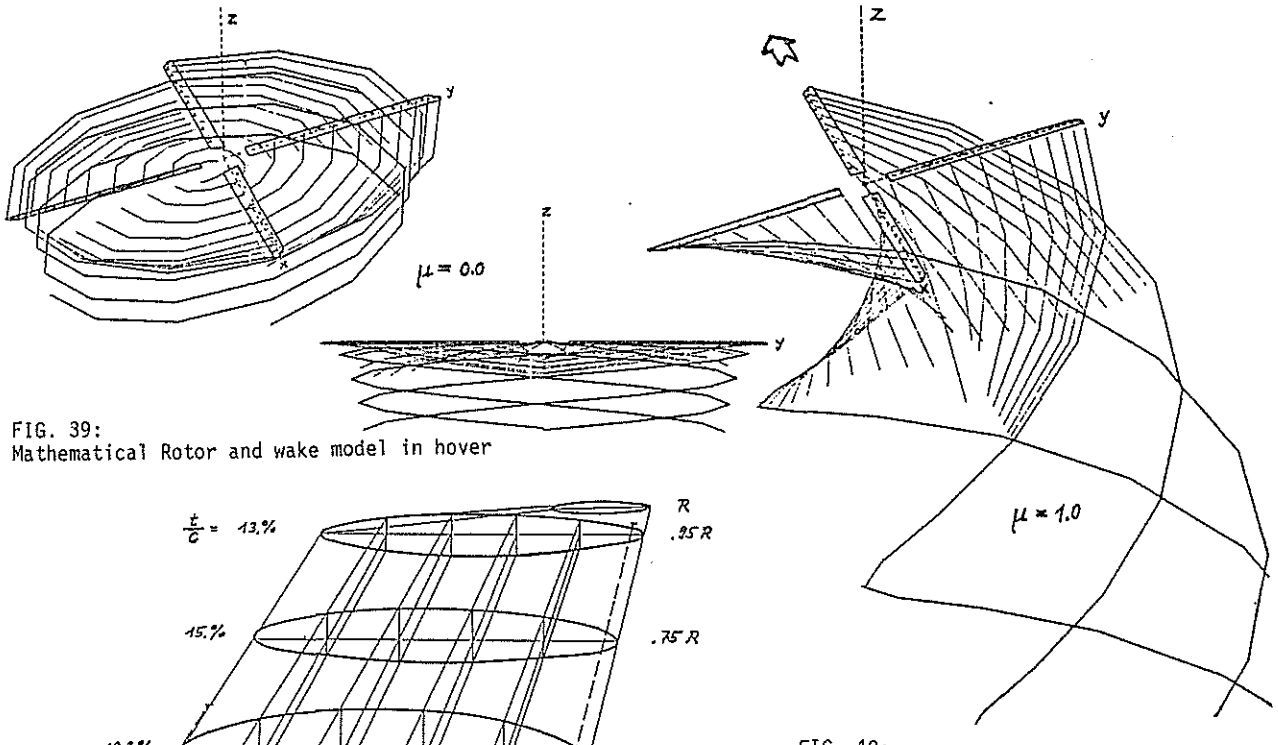

FIG. 39:
Mathematical Rotor and wake model in hover

FIG. 40:
Rotor wake model in fast forward flight

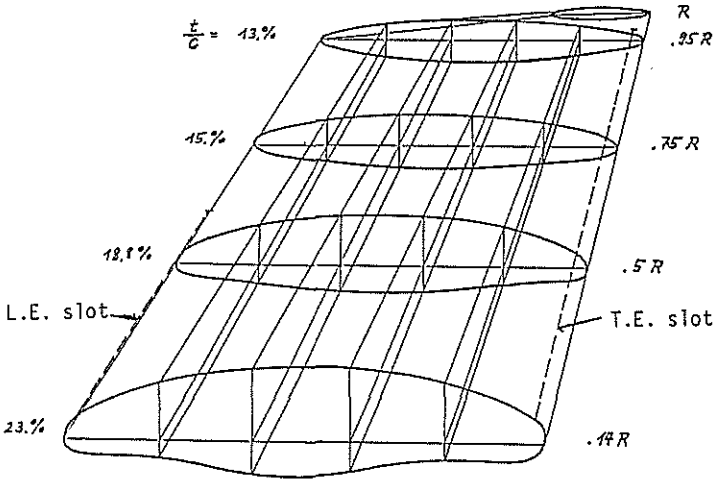

FIG. 41:
Efficient blade geometry for a fast CCR-Helicopter

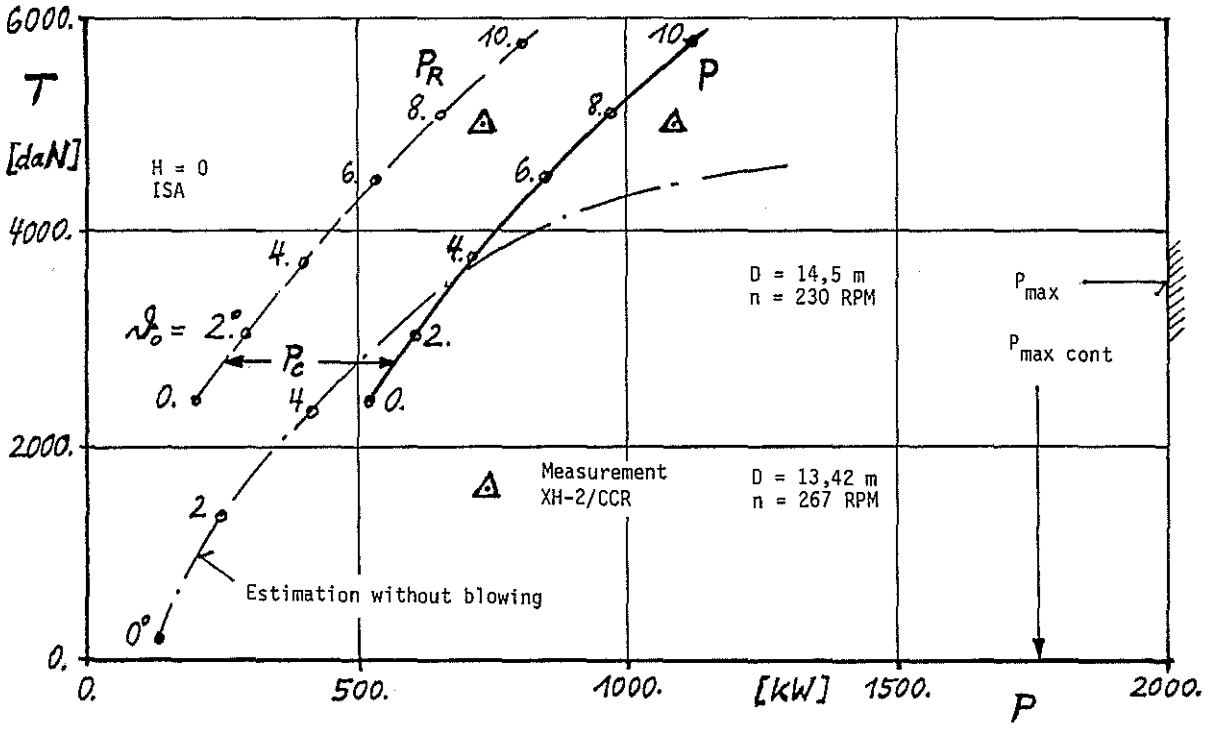

FIG. 42:
Rotor Shaft Power P_R and total required Power P (The sum of Shaft Power P_R and Compressor Power P_c) in dependence of pitch settings in hover

CONFIGURATION REQUIREMENTS

1500 KG PAYLOAD (INCL. 2 PILOTS)
A) 1000 KM RANGE
B) 2 x 30 MIN HOVER (MAX. RESIDUAL RANGE)
INSTALLED POWER 2 x 1000 KW

MANEUVRABILITY REQUIREMENTS

YAW VELOCITY IN HOVER	60°/SEC.
ACCELERATION FORWARD	0-100 KM/H ≤ 11,5 SEC
	0-150 KM/H ≤ 16,0 SEC
LATERAL ACCELERATION	0-40 KM/H ≤ 5,0 SEC
DECELERATION	110-0 KM/H ≤ 9,0 SEC

VELOCITY REQUIREMENT 250 KTS

FIG. 43:
Design requirements for the CCR-Application

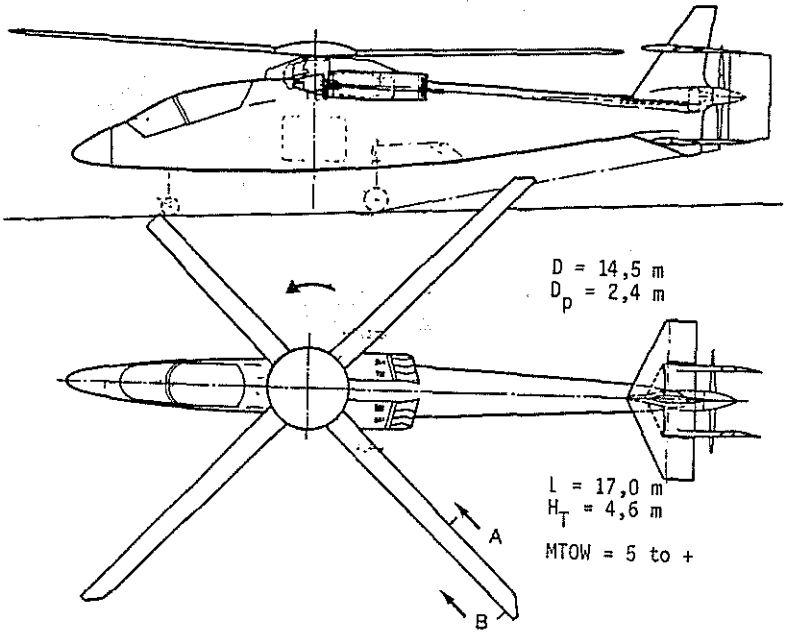

- Bearingless Flex Beam Rotor with Circulation Control and Mechanical Pitch Control
- Leading Edge Blowing (Partial Span) and Trailing Edge Blowing (Full Span)
- Higher Harmonic Control without Rotating Parts
- The Limitation of the Flight Regime to small Advance Ratios (Conventional Helicopter) is removed
- Propulsion by the Integrated Anti-Torque-Propulsor which enables High Speed Flight up to ~ 250 kts and enhances Acceleration and Deceleration Capabilities

FIG. 44: Design Features of the proposed CCR-Helicopter

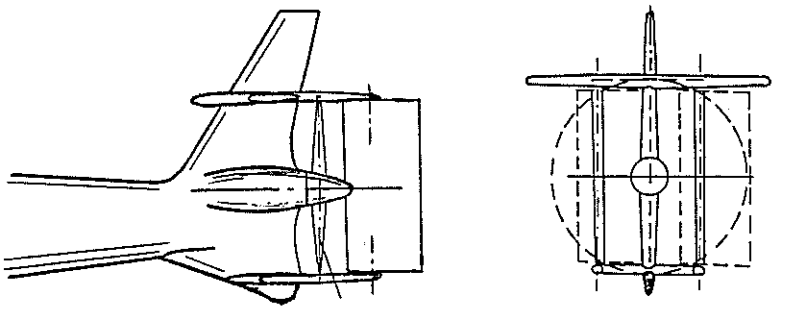

FIG. 45:
Layout of the Anti-Torque-Propulsor

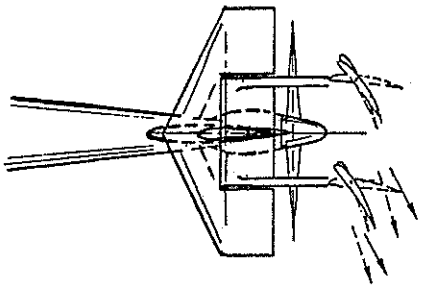

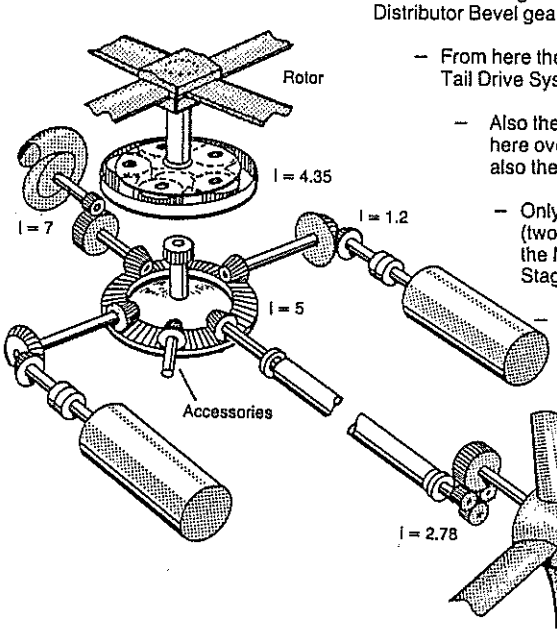

- The Engines are connected over shaft couplings and Nose Bevel gears to the Main Collector – Distributor Bevel gear Stage
- From here the Propulsor is driven by the Tail Drive System over a Reduction gear
- Also the Compressor is driven from here over a Single Stage gear and also the Accessories
- Only the remaining power (two thirds or less) enters the Main Rotor Gear, a Single Stage Planetary
- A Weight Saving Autorotation capable Design is possible

FIG. 46:
Design Features of the Drive System

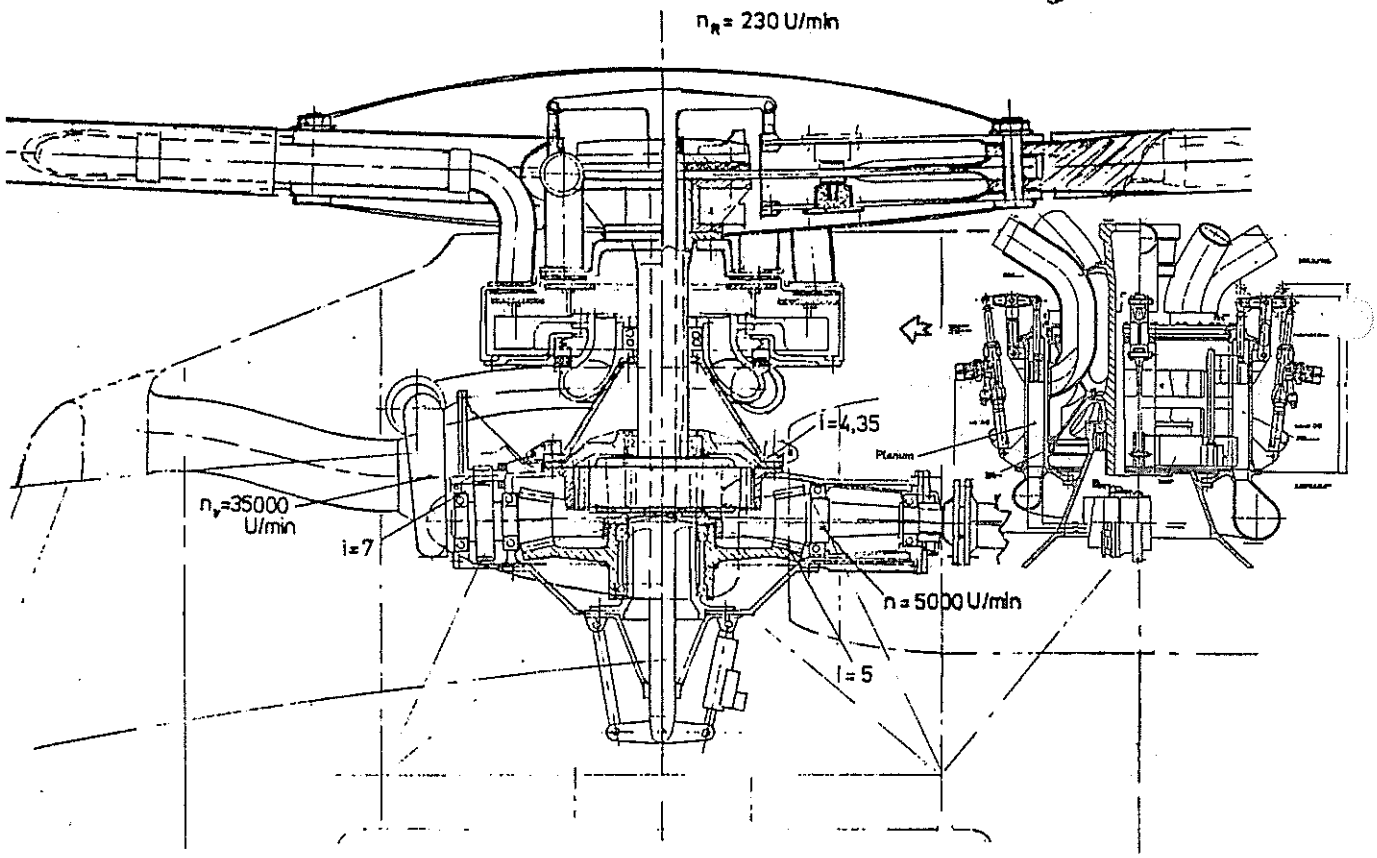

FIG. 47: Rotorhead, Pneumatic Control System, Main Rotor Gear Box

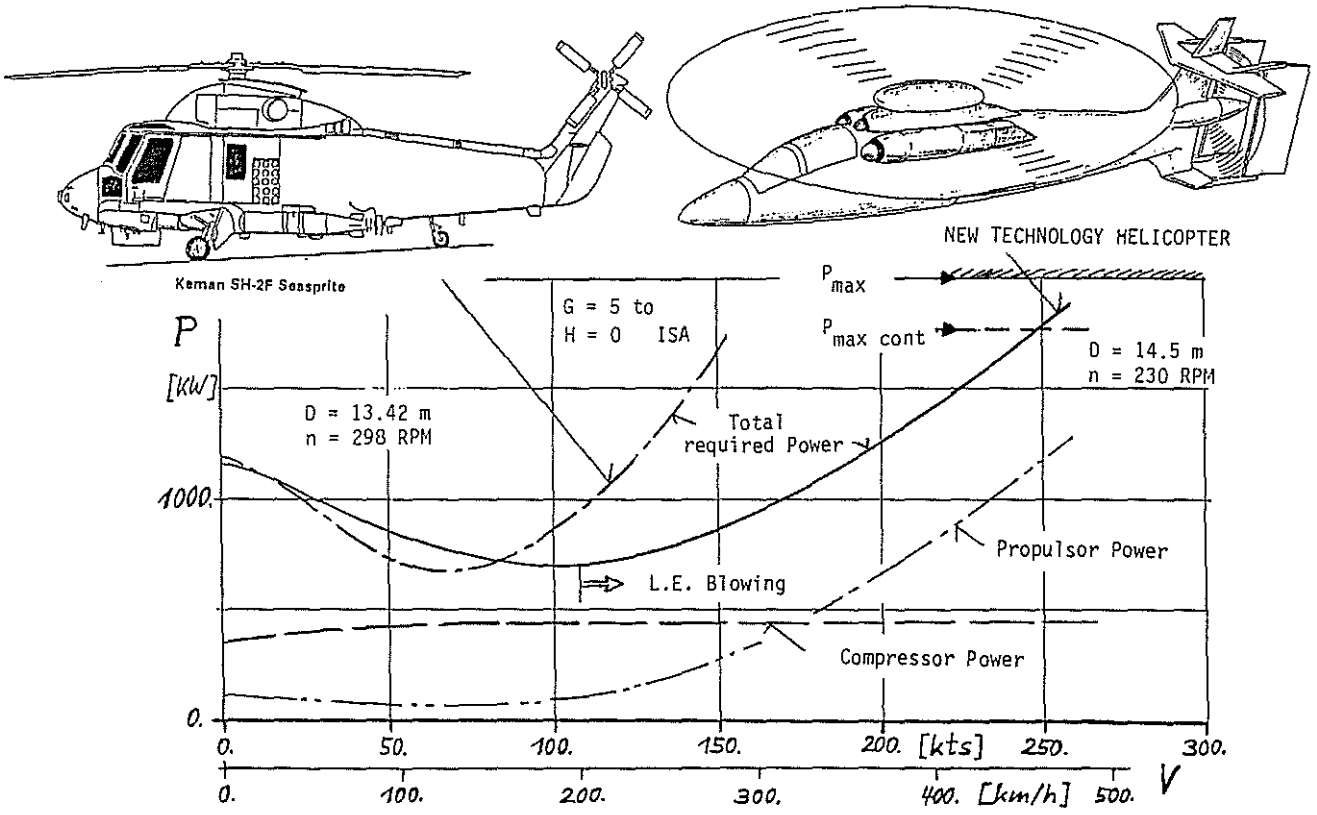

FIG. 48:
Comparison of the required power in dependence of flight speed of the proposed CCR-Helicopter with a conventional Helicopter of the came weight and the same installed power.

		A	B	C
	TAKE OFF WEIGHT [KG]	5000	5000	5250
	PAYLOAD [KG]	1300	1500	1500
A.	RANGE [KM]	1000	780	1000
	OR			
B.	HOVER TIME [MIN]	2 x 30	2 x 30	2 x 30
	RESIDUAL RANGE [KM]	700	520	700

(10 % TECHNOLOGY ADVANTAGE IN BASIC EMPTY WEIGHT)

FIG. 49:
Performance Summary

	REQU.	ROTOR TILT	PROPULSOR ALONE	COMBINATION
YAW VELOCITY [°/SEC]	60		60	
ACCELERATION FORWARD				
0 - 100 KM/H [SEC]	11,5	8,5	10,7	≤ 7
0 - 150 KM/H [SEC]	16,0	11,2	16,2	≤ 10
DECELERATION				
110 - 0 KM/H [SEC]	9.	≤ 9		≤ 9
LATERAL ACCELERATION				
0 - 40 KM/H [SEC]	5.	≤ 5		

FIG. 50:
Maneuvrability Summary